Electronic structure, thermodynamic and thermal properties of Ni-Al disordered alloys from LMTO-CPA-DFT calculations

1993 J. Phys.: Condens. Matter 5 1271

(http://iopscience.iop.org/0953-8984/5/9/012)

J. Phys.: Condens. Matter 5 (1993) 1271–1290. Printed in the UK

Electronic structure, thermodynamic and thermal properties of Ni–Al disordered alloys from LMTO–CPA–DFT calculations

I A Abrikosov†, A V Ruban†, D Ya Kats‡ and Yu H Vekilov†

† Department of Theoretical Physics, Moscow Institute of Steel and Alloys, 4 Leninskii Prospekt, Moscow, 117936, Russia

‡ All-Russia Institute of Aircraft Materials, 17 Radio Street, Moscow, 107005, Russia

Received 27 July 1992, in final form 8 December 1992

Abstract. The fast linear muffin-tin orbital coherent potential approximation method allied with density functional theory (LMTO–CPA–DFT) is used to calculate electronic structure and cohesive properties of Ni–Al random alloys on an underlying FCC lattice in all concentration intervals. Binding curves obtained in the calculations are used in the Debye–Grüneisen analysis to determine thermal properties and temperature-dependent Connolly–Williams cluster interactions. The calculated lattice constants, bulk moduli, enthalpies and free energies of formation are in good agreement with experiment. The globally and locally relaxed cluster interactions are compared with the results obtained from the total energy-band calculations for elements and ordered phases.

1. Introduction

Despite the considerable progress in *ab initio* calculations of electronic structures of solids, first-principles calculations of the thermodynamic properties of real systems may be done in limited cases. In particular, substantial difficulties arise for substitutional alloys with short-range order (SRO) effects. But even for completely disordered alloys first-principles calculations of thermodynamic properties are rare as yet, because of the computational cumbersomeness of ordinary (KKR–CPA) methods [1, 2].

Recently we proposed a fast version of the LMTO–CPA method [3] which reduces the computation time of electronic-structure calculations for random solid solutions down to that of the standard LMTO method for elements. Moreover, since our method is based on density functional theory, it is possible to study systems with considerable charge transfer and to calculate the energy properties of completely disordered alloys. In this paper we demonstrate the advantages of our method as applied to Ni–Al alloys.

These alloys constitute the basis of an important class of aircraft materials that have been actively studied, both experimentally and theoretically, for some decades. The main theoretical problem is the nature of interatomic interaction and the description of thermodynamic properties in the Ni–Al system. The first *ab initio* calculation of the electronic structure and cohesive properties of Ni–Al alloys was carried out by Hackenbracht and Kübler [4]. Using the ASW method in the density functional framework they obtained the magnetic moment and its pressure derivative, lattice constants, bulk modulus and the heats of formation of Ni_3Al, NiAl and Al_3Ni compounds. Furthermore, in an attempt to isolate the dominant bonding

0953-8984/93/091271+20$07.50

forces, they decomposed the heats of formation into site- and angular-momentum contributions. In contrast to Miedema's semiempirical theory [5], which ascribes the prominent contribution to the enthalpy of formation to the p–d hybridization term, they concluded that the main binding term for Ni_3Al arises from the d electrons of Ni; for NiAl the d electrons of Al and Ni provide the leading terms; for Al_3Ni the dominant role is played by the p and d electrons of Al.

However, the last conclusion gives rise to doubts because the site-and angular-momentum decompositions in their work arise from the similar decomposition of the electronic pressure. But the absence of hybridization terms in this scheme is an artifact of the theory. Therefore, in this case, further analysis of local and partial densities of states is desirable.

Another way of considering interatomic interactions, which facilitates not only the interpretation of experimental data but also the calculation of various physical properties, is based on the determination of interatomic potentials. In the first-principles methods, such potentials cannot be derived explicitly, but this can be done unambiguously in the model pseudopotential method by means of the perturbation theory.

However, first-principles calculations may be used for determination of the potential on the fixed lattice, which is necessary for calculations of the configurational effects on this lattice in thermodynamic properties. In this case, the total energies of a number of atomic configurations are calculated by the *ab initio* method, after which the Connolly–Williams procedure is used for matching calculated total energies to their phenomenological expression in terms of the multisite interactions [6].

This method was applied to the Ni–Al system for the first time by Carlsson and Sanchez [7–9]. They calculated various thermodynamic properties of the system, in particular its phase diagram on an underlying FCC lattice. Although the shape of the Ni-rich part of the calculated phase diagram agrees fairly well with experimental observations, the transition temperature is roughly 40% too high and correspondingly the free energy is 40% too low. Since in their work Carlsson and Sanchez [8] used only two elements and three ordered phases (Ni, Ni_3Al, NiAl, Al_3Ni and Al in the structures A1, $L1_2$, $L1_0$) for the representation of all possible atomic configurations in alloys, the question arises as to whether potentials derived in this way are applicable to random alloys. Pasturel *et al* have partially touched upon this question in their recent paper [10]. In addition to the above three structures they calculated the energies of the DO_{22} structure for both Ni_3Al and $NiAl_3$ phases. In the tetrahedron approximation of the Connolly–Williams method this structure displays the same correlations as the $L1_2$ structure; their energies must, therefore, be degenerate. Though the difference for both phases is about 2 kJ mol^{-1} ($\simeq$ 250 K), it does not prove the convergence of the tetrahedron approximation in the Connolly–Williams method for the Ni–Al system. In the paper of Lu and co-workers [11] where ten different structures were used in the Connolly–Williams method there are some deviations of cluster interactions from the results of Carlsson and Sanchez. Moreover, the question still remains of what the electronic structure of random Ni–Al alloys is like.

In our work we attempt to shed light on these points using the previously proposed fast LMTO–CPA method allied with the density functional theory.

The organization of this paper is as follows. In section 2 we outline the LMTO–CPA method. In section 3 we present details of the calculation and discuss the results for the electronic structure of Ni–Al random alloys. To evaluate the temperature

dependence of equilibrium lattice separations, coefficients of thermal expansion and bulk moduli, in section 4, we use Debye–Grüneisen analysis following Moruzzi [12, 13]. In section 5 we determine locally and globally relaxed multisite interactions and the thermodynamic properties of Ni–Al alloys using the Connolly–Williams method. In section 6 we present the Ni-rich part of the calculated phase diagram and compare it with available experimental and theoretical results. In section 7 we summarize our conclusions.

2. The fast LMTO–CPA–DFT method

The formulation of the CPA equations in the multiple-scattering scheme is most convenient for the scattering path operator τ (KKR–CPA method [14,15]) or for the analogous 'little' Green function g of the LMTO method (in this paper we use the notations of [16]). In the single-site CPA, a multicomponent disordered alloy is replaced by an ordered system of effective scatterers with the same coherent potential function $\tilde{P}$. The latter must be determined from the self-consistent CPA equations. The coherent Green function $\tilde{g}$ for this system can be calculated as a Green function of an ideal crystal [16]

$$\tilde{g}^{\alpha}_{RL,R'L'}(E) = (V_{BZ})^{-1} \int_{V_{BZ}} dk\, e^{ik\cdot(R-R')} \{[\tilde{P}^{\alpha}(E) - S^{\alpha}(k)]^{-1}\}_{RL,R'L'}. \tag{1}$$

Here V_{BZ} is the Brillouin zone volume; $S_{RL,R'L'}$ the matrix of structure constants, which contains all information about the atomic positions; and α denotes the LMTO representation [17]. The subscripts are the RL matrices, where R is the radius vector of an atom in the unit cell, and L is the common notation for the angular (l) and magnetic (m) quantum numbers. The evident E-dependence will hereinafter be omitted except in special cases.

The CPA condition consists in the absence of electron scattering, on the average, by the alloy components which are randomly distributed in the effective lattice

$$\sum_i c_i \mathbf{g}^{i\alpha} = \tilde{\mathbf{g}}^{\alpha} \tag{2}$$

where i denotes the alloy components, c_i are their concentrations and $\mathbf{g}^{i\alpha}$ is the Green function of the ith impurity in the ideal effective crystal. Such a Green function can be found from the Dyson equation [16]

$$\mathbf{g}^{i\alpha} = [(\tilde{\mathbf{g}}^{\alpha})^{-1} + \mathbf{P}^{i\alpha} - \tilde{\mathbf{P}}^{\alpha}]^{-1}. \tag{3}$$

In this equation $\mathbf{P}^{i\alpha}$ is the usual LMTO potential function for the alloy component i. This is determined by solving the Schrödinger (or Dirac) equation for a single atomic sphere i. Moreover, this function can be parameterized

$$P^{i\alpha}_{RL}(E) = (E - C^{i}_{RL})/[(E - C^{i}_{RL})(\gamma^{i}_{RL} - \alpha_L) + \Delta^{i}_{RL}] \tag{4}$$

and the potential parameters C, γ and Δ are obtained by solving the Schrödinger equation for only one value of energy E_ν [17].

From equations (2) and (3) we obtain the main LMTO–CPA equation

$$\sum_i c_i[(\tilde{\mathbf{g}}^\alpha)^{-1} + \mathbf{P}^{i\alpha} - \tilde{\mathbf{P}}^\alpha]^{-1} = \tilde{\mathbf{g}}^\alpha. \tag{5}$$

Equations (1) and (5) must be solved simultaneously. The traditional way of solving such systems consists in the step by step iteration procedure: the initial value of $\tilde{P}$ (for example, $\tilde{\mathbf{P}}^\alpha = \sum_i c_i \mathbf{P}^{i\alpha}$) is used for the Brillouin zone integration in equation (1) and the resulting value of $\tilde{g}$ is used for the coherent-potential function recalculation by equation (5). This procedure is carried out until consistency between the input and output coherent potential functions is attained.

This is a very time-consuming scheme, because we must fulfil $\simeq 20$ iterations for any energy point. This great price is the main limiting factor for all methods based on the CPA.

We overcome these difficulties by using the method of k-space integration over the Weyl uniform mesh [18] which allows one to carry out the self-consistent determination of the coherent-potential function simultaneously with the integration procedure. Indeed, if the k-points are distributed randomly in the Brillouin zone (or in its irreducible part), the integral of the periodic function $f(k)$ may be replaced by the sum

$$(V_{\mathrm{BZ}})^{-1} \int_{V_{\mathrm{BZ}}} f(k)\mathrm{d}k = \lim_{N\to\infty} N^{-1} \sum_{n=1}^{N} f(k_n). \tag{6}$$

From equations (1) and (6) we obtain the following recurrent scheme

$$\tilde{\mathbf{g}}_n^\alpha = (1 - 1/n)\tilde{\mathbf{g}}_{n-1}^\alpha + (1/n)[\tilde{\mathbf{P}}^\alpha - \mathbf{S}^\alpha(k_n)]^{-1}. \tag{7}$$

Then, we can modify $\tilde{P}$ by adding any new k-point and solving equation (5) for $\tilde{g}_n$. Therefore, equation (5) takes the form

$$\sum_i c_i[(\tilde{\mathbf{g}}_n^\alpha)^{-1} + \mathbf{P}^{i\alpha} - \tilde{\mathbf{P}}_n^\alpha]^{-1} = [(\tilde{\mathbf{P}}_{n+1}^\alpha - \tilde{\mathbf{P}}_n^\alpha) + (\tilde{\mathbf{g}}_n^\alpha)^{-1}]^{-1} \tag{8}$$

which is equivalent to equation (5) for $n \to \infty$ provided $\lim_{n\to\infty} \tilde{P}_n^\alpha = \tilde{P}^\alpha$. Finally, the system of LMTO–CPA equations takes the form

$$\begin{aligned} \tilde{\mathbf{g}}_n^\alpha &= (1 - 1/n)\tilde{\mathbf{g}}_{n-1}^\alpha + (1/n)[\tilde{\mathbf{P}}_{n-1}^\alpha - \mathbf{S}^\alpha(k_n)]^{-1} \\ \tilde{\mathbf{P}}_{n+1}^\alpha &= \tilde{\mathbf{P}}_n^\alpha + \beta\left\{\left(\sum_i c_i[(\tilde{\mathbf{g}}^1 + \mathbf{P}^{i\alpha} - \tilde{\mathbf{P}}_n^\alpha]^{-1}\right) - (\tilde{\mathbf{g}}_n^\alpha)^{-1}\right\} \end{aligned} \tag{9}$$

where $\beta \leqslant 1$ is the mixing coefficient which stabilizes the iteration procedure.

Using this method, only one Brillouin zone integration is required for the determination of the Green function at each energy point. Therefore, our method is fast and efficient.

Once the system of equations (9) has been solved, the alloy components of the Green functions $g^{i\alpha}$ can be obtained from equation (3), following which the density of states can be constructed as

$$N_l(E) = \sum_i c_i N_l^i(E). \tag{10}$$

Here N_l^i is the local partial density of states, for which the usual LMTO expansion [15] is used

$$N_l^i(E) = (-2\pi)^{-1}\dot{P}_l^{i\alpha}(E)\sum_m \operatorname{Im} g_{lm,lm}^{i\alpha}(E). \tag{11}$$

In equation (11) $\dot{P}_l^{i\alpha}(E)$ is the energy derivative of the potential function.

Moreover, we can also ensure charge DFT self-consistency. The validity of this procedure for disordered alloys within the CPA was accurately proved in [1]. The electronic charge of the alloy components $n^i(r)$ is calculated as

$$n^i(r) = n_c^i(r) + \int_{E_b}^{E_F}\sum_l N_l^i(E)[\phi_l^i(E,r)]^2\,\mathrm{d}E \tag{12}$$

where n_c^i is a core charge density, E_b the bottom of the valence band, E_F the Fermi energy and ϕ is a radial wave function inside the atomic sphere [16]. The potentials of the alloy components must be constructed 'independently' from one another (all the effects connected with the existence of the solid solution are included in $\bar{g}$ and therefore g^i).

Knowing the self-consistent charge density, the total ground-state energy of an alloy and its thermodynamic properties can be calculated. The usual DFT expansion for E_{tot} has the form

$$E_{tot} = \int_{-\infty}^{E_F}\mathrm{d}E\,EN(E) - \int \mathrm{d}r\,n(r)v(r) + \frac{1}{2}e^2\iint \mathrm{d}r\,\mathrm{d}r'\,\frac{n(r)n(r')}{|r-r'|}$$
$$- e^2\sum_i Z_i\int \mathrm{d}r\,\frac{n(r)}{|r-R_i|} + E_{xc}\{n(r)\} + \frac{1}{2}e^2\sum_{i\neq j}\frac{Z_iZ_j}{|R_i-R_j|} \tag{13}$$

where $v(r)$ is the self-consistent potential, r and R the electronic and nuclear radius vectors, respectively, Z_i the nuclear charge and E_{xc} the exchange–correlation energy.

The electron gas pressure P and bulk modulus B are defined as

$$P = -\mathrm{d}E_{tot}/\mathrm{d}\Omega \qquad B = -\Omega\mathrm{d}P/\mathrm{d}\Omega|_{\Omega=\Omega_0} \tag{14}$$

Here Ω is the system volume and Ω_0 the equilibrium lattice volume which can be obtained from the condition $P(\Omega_0) = 0$.

For the ground-state energy of the disordered alloy we can use the expression [1]

$$E_{tot}^{alloy} = \sum_i c_i E_{tot}^i \tag{15}$$

where E_{tot}^i are defined by (13). It is easy to show from (14) and (15) that the electron gas pressure

$$P^{alloy} = \sum_i c_i P^i. \tag{16}$$

3. Details of calculation and electronic structure of disordered Ni–Al alloys

We used 500 k-points in the 1/48 part of the FCC Brillouin zone to solve the system of LMTO–CPA equations (9). The k-mesh was constructed in accordance with Akai [18]. As was shown in his paper, the accuracy of the total energy calculation for such a k-point distribution is of the order of 0.1 mRyd, which is sufficient for the total energy calculations.

All calculations were done with $l_{max} = 3$, instead of as in our previous paper [19], where $l_{max} = 2$ was used. As we will show in section 4, better agreement between the experimental and theoretical values of lattice parameters is obtained in this case. Here we must point out that if l_{max} is equal to 3 the coherent Green function and the effective potential function are non-diagonal matrices even for cubic crystals, because the irreducible representation Γ^{15} appears for both p and f electrons. However, in our case these non-diagonal p–f elements are fortunately much smaller than any others. Moreover, we are interested only in the diagonal elements of the Green functions of alloy components (see equation (11)), and, as can easily be shown, the influence of non-diagonal elements on the diagonal ones is of the next order of magnitude, so they can be omitted with only a small decrease in accuracy.

Describing other details of the calculations, we would like to point out that all energy integrals were calculated in the complex energy plane [20]. A rectangular contour with 35 energy points and with an imaginary part equal to 0.3 Ryd was used for this purpose.

We constructed the exchange–correlation potential in the local-density approximation (LDA) within the Perdew–Zunger interpolation term [21]. Core states were recalculated at all LDA interations.

In our calculations we usually used the LMTO [17] representation with $\alpha = 0$. But sometimes the convergence was very poor because of some peculiarities of the potential-function energy dependence (especially for the $Ni_{25}Al_{75}$ alloy, where such a peculiarity for the $\alpha = 0$ LMTO representation exists near the Fermi energy). In this case, some other LMTO representation can be employed (we have used $\alpha_l = \gamma_l^{Al}$, where γ is the potential parameter) in order to remove the peculiarity outside the energy region of interest.

The resultant density of states for an Al impurity in Ni (dilute alloy), completely disordered $Ni_{92}Al_8$, $Ni_{86}Al_{14}$, $Ni_{75}Al_{25}$ and Ni_3Al compounds are presented in figures 1–5.

Note that the spectra of the dilute alloy and the stoichiometric compound on the one hand and the spectra of disordered alloys on the other, are rather different.

We can point out that for the dilute alloy and for Ni_3Al strong hybridization between the p electrons of Al and the d electrons of Ni is observed in the energy region from -0.15 to -0.35 Ryd below E_F. This hybridization consists in correlation between the positions of the Al p peaks and the Ni d peaks. Moreover, d–d hybridization in the energy region from -0.05 to -0.15 Ryd is also observed. Therefore we can speak about the covalency of chemical bonds between the Al atoms and their nearest 12 Ni neighbours ($L1_2$ type structure for Ni_3Al and a single impurity in the FCC lattice for the dilute alloy).

In completely disordered concentrated Ni–Al alloys Al atoms are surrounded by both Ni and Al atoms. All peaks in local state densities are smeared out and hence only weak hybridization is observed. Therefore the local configuration $AlNi_{12}$ leads to the strong hybridization of the electronic structure. The latter stabilizes

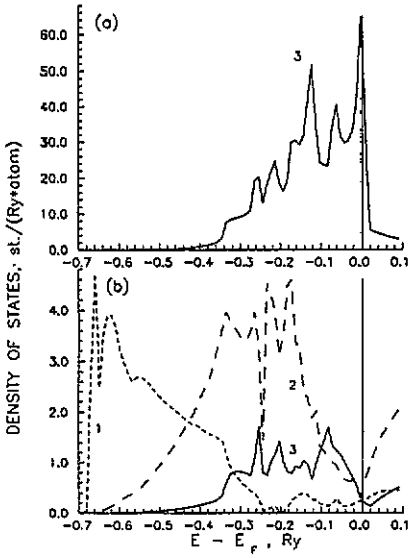

Figure 1. Local densities of states (DOS) for Al impurity in Ni. (*a*) Partial DOS on the Ni atom, (*b*) partial DOS on the Al atom. (1) s, (2) p and (3) d electrons.

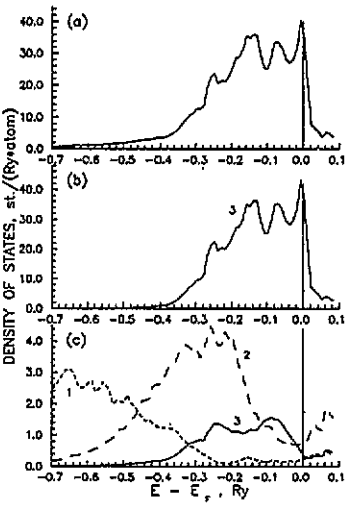

Figure 2. The density of states for $Ni_{92}Al_8$. (*a*) Total DOS, (*b*) partial DOS on the Ni atom, (*c*) partial DOS on the Al atom. (1) s, (2) p and (3) d electrons.

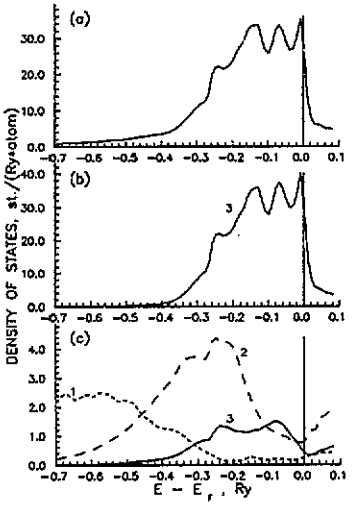

Figure 3. The density of states for $Ni_{86}Al_{14}$. (*a*) Total DOS, (*b*) partial DOS on the Ni atom, (*c*) partial DOS on the Al atom. (1) s, (2) p and (3) d electrons.

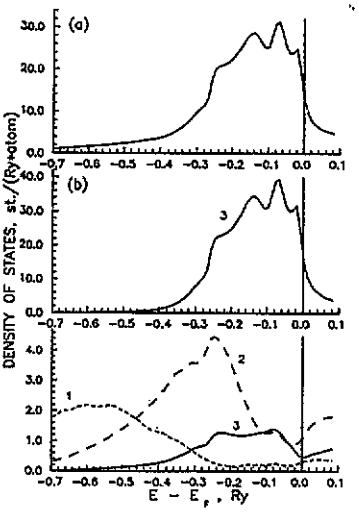

Figure 4. The density of states for $Ni_{75}Al_{25}$. (*a*) Total DOS, (*b*) partial DOS on the Ni atom, (*c*) partial DOS on the Al atom. (1) s, (2) p and (3) d electrons.

the corresponding atomic structure (as will be shown in section 5, the enthalpy of formation for Ni_3Al is lower than the mixing enthalpy for the $Ni_{75}Al_{25}$ alloy). From this point of view, strong SRO effects in the Ni–Al system can be also explained by the tendency of Al atoms to be surrounded by Ni in Ni-rich alloy.

The resulting spectra for Al-rich Ni–Al alloys and for the equiatomic alloy $Ni_{50}Al_{50}$

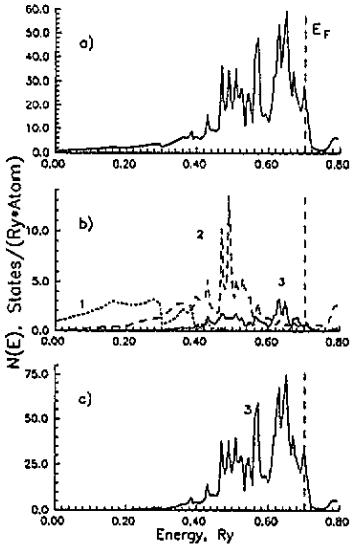

Figure 5. The density of states for Ni_3Al. (*a*) Total DOS, (*b*) partial DOS on the Ni atom, (*c*) partial DOS on the Al atom. (1) s, (2) p and (3) d electrons.

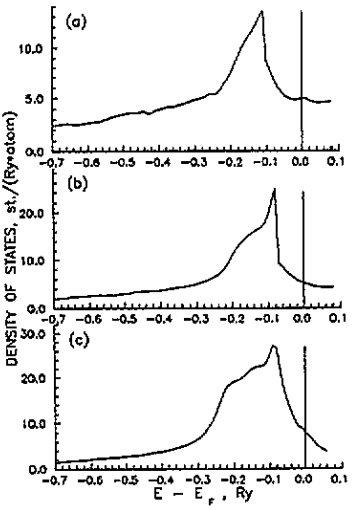

Figure 6. Total densities of states for equiatomic and Al-rich alloys. (*a*) Ni_8Al_{92}, (*b*) $Ni_{25}Al_{75}$, (*c*) $Ni_{50}Al_{50}$.

are presented in figure 6. It is well known that for an Ni impurity in Al, a virtual bound 3d state exists at an energy $\simeq 0.15$ Ryd below E_F [22,23]. For completely disordered concentrated Al-rich alloys such a state is also observed (see figure 6(*a*)). It is widened and displaced to the Fermi level with an increase in Ni concentration, and the Ni-like d band is gradually formed from this virtual state.

Another important characteristic of the electronic structure is charge transfer. It is obvious that the difference between the structure of Ni and Al electronic valence shells must lead to substantial charge transfer in Ni–Al alloys. Unfortunately, there is no single way to determine charge transfer because it is impossible to divide the crystal unambiguously into regions related to each atom.

However, in the ASA we may observe the general tendencies of charge transfer if we use the same Wigner–Seitz radius ratio for different atoms in all compositions. In this case, charge transfer is defined mostly as the difference between the number of electrons in an isolated atom and the corresponding Wigner–Seitz sphere in a solid.

On the other hand, in the ASA there is an additional relationship between the values of charge transfer Δq_i for different atoms

$$\sum_i c_i \Delta q_i = 0 \tag{17}$$

where c_i is the atomic fraction of atoms of i-type. It is easy to show that equation (17) leads to the 'unnatural' concentration dependency of Δq_i. In particular, $\Delta q_i \to 0$ when $c_i \to 1$ independently of the values of Δq_j $(j \neq i)$. Therefore, there is no reason to compare Δq_i for alloys with different composition.

Nevertheless, this difficulty with the definition may easily be overcome in the following way. Let us consider a two-component alloy (for a many-component alloy this can be done in the same manner). We may define $\Delta q_A(c)$, where $c \equiv c_A$, as

$$\Delta q_A(c) = 2(1-c)\Delta\tilde{q}(c). \tag{18}$$

Here we introduce a new function $\Delta\tilde{q}(c)$. By substituting equation (18) in equation (17) we obtain

$$\Delta q_B(c) = -2c\Delta\tilde{q}(c). \tag{19}$$

Since $\Delta\tilde{q}(c)$, in contrast to $\Delta q_i(c)$, does not depend on the type of atom and may be an arbitrary function of c, it is very convenient to choose it as the definition of charge transfer.

In table 1 we show the values of $\Delta\tilde{q}$ for Ni–Al alloys. We see that in this system the normalized charge transfer $\Delta\tilde{q}(c)$ depends very slightly on the concentration. In contrast, the atomic configuration of the alloy has considerable influence over the value of charge transfer: $\Delta\tilde{q}(c)$ for the ordered Ni_3Al is about twice as great as for the disordered $Ni_{75}Al_{25}$ alloy.

Table 1. The charges of the Ni and Al atomic spheres (Δq_{Ni} and Δq_{Al}) and normalized charge transfer $\Delta\tilde{q}$ for Ni–Al alloys.

Alloys	Δq_{Ni}	Δq_{Al}	$\lvert\Delta\tilde{q}\rvert$
Al impurity in Ni	0.0	0.450	0.225
Ni_3Al	−0.162	0.488	0.325
$Ni_{92}Al_8$	−0.021	0.246	0.134
$Ni_{75}Al_{25}$	−0.068	0.203	0.135
$Ni_{50}Al_{50}$	−0.137	0.137	0.137
$Ni_{25}Al_{75}$	−0.203	0.068	0.135
Ni_8Al_{92}	−0.246	0.021	0.134

Table 2. Partial decomposition of the valence electrons in Al and Ni Wigner–Seitz spheres for random Ni–Al alloys.

c_{Al} (at.%)	Al				Ni			
	s	p	d	f	s	p	d	f
8	0.95	1.314	0.400	0.09	0.673	0.766	8.499	0.083
25	0.959	1.358	0.398	0.081	0.671	0.784	8.541	0.074
50	0.981	1.418	0.397	0.066	0.673	0.812	8.592	0.059
75	1.029	1.446	0.403	0.055	0.684	0.820	8.648	0.049
92	1.070	1.450	0.412	0.048	0.695	0.812	8.693	0.042

The partial decomposition of the charge in the Al and Ni Wigner–Seitz spheres is presented in table 2. For the same reason as for Δq_i there is no sense in comparing these values for different concentrations. Therefore we cannot directly relate these results and the experimental charge transfer data [24] in which an increase in the number of Ni d electrons was found only in the interval from 0 to 50 at.% Al. However, considering the relative position of the Ni-like d band and the Fermi level at different concentrations of Al (figures 1–5), we point out that the latter shifts toward the Ni d-band edge with increase of Al concentration. So the unoccupied part of this band decreases and for $Ni_{50}Al_{50}$ alloy it is practically full. This indirectly agrees well with the experiment.

4. Thermal properties of Ni–Al alloys

The possibility of local-density functional band-structure self-consistency in the framework of the CPA [1,2] reveals the way to the direct calculations of thermodynamic and thermal properties of disordered alloys. These properties may also be obtained with the help of the Connolly–Williams method (CWM) [6] from the set of total-energy band calculations of elements and ordered compounds. However, first, such calculations are highly cumbersome and, second, the question of convergence of the CWM [25] also arises because it is not clear beforehand how sensitive the system is to changes in its atomic configuration.

For Ni–Al alloys, the CWM was employed by Carlsson and Sanchez to calculate the effective pair interaction (EPI) [7], free energy of formation, phase diagram [8], and other thermodynamic properties [9], and recently by Pasturel *et al* [10] and Lu *et al* [11] for phase diagram calculation. All these works (with the exception of [11]) were carried out in the tetrahedron truncation of cluster interactions, leading to a set of five interactions obtained from a set of total energies of two elements (Al and Ni) and three compounds (Al_3Ni, AlNi, Ni_3Al). Despite some discrepancies between calculated and experimental data (for instance, in the transition temperatures and free energy of formation [8]), Carlsson and co-workers did not verify the sufficiency of tetrahedron truncation in the CWM for this system. In order to clear up this question in particular we decided to employ the CWM also with tetrahedron truncation but on the basis of the total energies of completely disordered solid solution for thermodynamic calculations. Apart from that, the CWM allows us to take into account short-range order (SRO) effects which are sufficiently strong in Ni–Al alloys.

Since in the calculation of thermal properties, accuracy in obtaining the binding curves is very important, we have done calculations for a set of five values of lattice parameters with step size $\simeq 0.1$ au in the vicinity of the equilibrium value for each concentration of Al (8, 25, 50, 75, and 92 at.%). In this case, as can easily be seen, the regions of total-energy definition for different concentrations were found to be separated from one another. Therefore, to avoid mistakes in the extrapolation of the binding-energy curves for alloys with different concentrations on the same lattice constants, the Rose–Smith universal function [26] was used. This function is convenient because it is uniquely defined by parameters corresponding to the equilibrium state.

As a basis for the analytical expression of the Rose–Smith curve the function defined in [27] was chosen:

$$E_{tot}(a^*) = \begin{cases} E_\infty + E_s(1+a^*)e^{-a^*} & a^* > 0 \\ E_\infty + E_s\left(1 + \dfrac{a^*}{(1+\lambda a^*)^2} + 2\lambda a^{*2}\right)e^{-a^*} & a^* < 0 \end{cases} \tag{20}$$

$$a^* = (1/\lambda)[a/a_0 - 1] \qquad \lambda = [-E_s/9B_0\Omega_0]^{1/2}$$

where a_0, B_0, Ω_0, and E_s are the equilibrium lattice constant, bulk modulus, equilibrium atomic volume and cohesive energy, respectively. E_∞ is the energy of the system with the atoms removed one from another to infinity.

However, in the determination of the thermal properties the function (20) turned out to be inconvenient because of the gap in the third derivative $E_{tot}(a^*)$ at $a^* = 0$, which leads to trouble in the definition of the Grüneisen constant [10]. Therefore in

equation (20), additional terms smoothing the third derivative were included:

$$\begin{cases} 3(1+\delta)\lambda^2 a^{*2} e^{-a^*} & a^* > 0 \\ 3\delta\lambda^2 a^{*2} e^{-a^*} & a^* < 0 \end{cases} \qquad (21)$$
$$\delta = (3\lambda\gamma - 9\lambda^2 - 1)/9\lambda^2.$$

Here γ is the Grüneisen constant.

The parameters of the Rose–Smith curve corresponding to the ground-state properties of the disordered alloys are summarized in table 3.

Table 3. The equilibrium lattice parameter, bulk modulus, and Grüneisen constants derived from LMTO–CPA–DFT calculations for disordered Ni–Al alloys on an FCC lattice.

c (at.% Al)	a_0 (au)	B_0 (kbar)	γ
8	6.657	2285	2.22
25	6.737	2007	2.13
50	6.930	1565	1.98
75	7.213	1173	2.19
92	7.450	923	2.25

To take into account the phonon contribution we used the Debye–Grüneisen model following Moruzzi and co-workers [12, 13]. However we corrected this model by including the temperature dependence of the Grüneisen constant, which increases in comparison with its low-temperature value approximately by $\frac{1}{3}$ at one third of the Debye temperature θ_D [28]

$$\gamma(T) = \gamma_{LT} + \tfrac{2}{3} f/(1+f) \qquad f = \exp(-\theta_D/3T) \qquad (22)$$

where [10]

$$\gamma_{LT} = -1 - (\Omega/2)(\partial^2 P/\partial\Omega^2)/(\partial P/\partial\Omega) \qquad \theta_D = 41.63[RB/M]^{1/2} \qquad (23)$$

and M is the atomic weight.

In figure 7 we show the calculated room-temperature lattice parameters and bulk moduli for disordered Ni–Al alloys after Debye–Grüneisen analysis of the binding curves. First of all it is necessary to note that taking into consideration the f electrons leads to both a decrease in the calculated lattice parameters and an increase in the bulk moduli in comparison with the results of our previous work [19]. The analogous effect of including high-l components in the calculation was also observed in [1]. It can easily be seen from figure 7 that there is some deviation of the concentration dependences of the calculated lattice constants and bulk moduli from the experimental data [29–35]. In particular, the theoretical values of the lattice parameters increase with Al concentration more quickly than the corresponding experimental ones and *vice versa* (the calculated bulk moduli fall more rapidly than the experimental values). In our opinion, this divergence is the consequence of the actually existing SRO effects in the Ni–Al alloys which were not taken into account in the theoretical calculations.

In figure 8 we show the calculated room-temperature coefficients of thermal expansion for the Ni-rich region where it makes sense to compare them with available

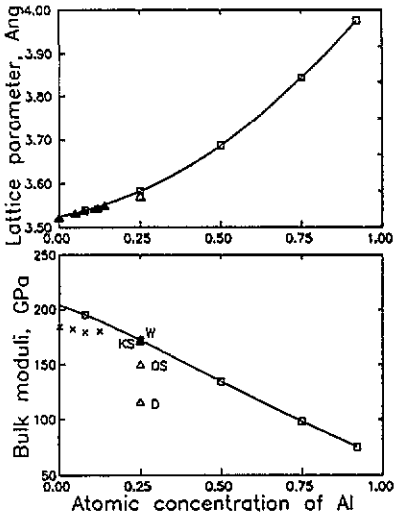

Figure 7. Room-temperature equilibrium lattice constants and bulk moduli for Ni–Al alloys. □ denotes calculated values. ▲ denotes the experimental data for lattice constants of Ni–Al solid solutions [29] and Δ denotes the experiment for Ni_3Al [30]. + denotes the experimental bulk moduli of Ni-rich alloys [31]) and Δ denotes the experimental data for Ni_3Al: OS, D, KS and W come from [32], [33], [34] and [35] respectively.

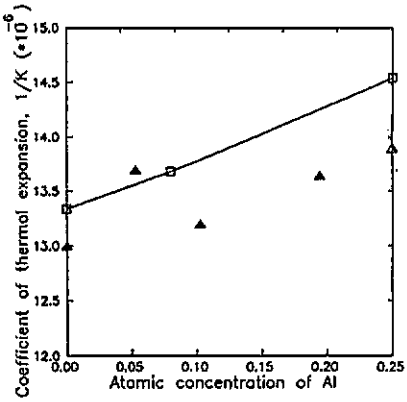

Figure 8. Room-temperature coefficients of thermal expansion for Ni-rich alloys. The values for pure Ni were calculated from the binding curve obtained with the help of the Conolly–Williams method. Experimental values are denoted by ▲ from [30] and by Δ from [36].

experiments [36,30]. On the whole, the slight tendency for the coefficients obtained in calculation to grow with Al concentration agrees well with the experimental data. However, it should be noted that there is too great a dispersion of the latter. In addition, for real alloys a peculiarity in the concentration dependence of the thermal expansion must be observed when caused by the transition from ferromagnetic (low Al concentration) to paramagnetic alloys (high Al concentration). It is obvious that these effects cannot be reproduced in our spin-restricted calculations.

5. Multisite interactions and thermodynamic properties of Ni–Al alloys

Knowing the binding energy curves for five concentrations of Al (8, 25, 50, 75, and 92 at.%) as a function of volume and temperature, we used the CWM for the determination of configuration- and concentration-independent potentials (interactions) on the tetrahedron of the FCC nearest-neighbour sites from the set of equations

$$E_{\text{tot}}(c,T) = \sum_{n=0}^{4} V_n(T)\xi_n(c) \tag{24}$$

where V_n is the n-body temperature-dependent interaction, and ξ_n is the correlation function which is given by $\xi_n(c) = (2c-1)^n$ for a completely disordered alloy (here we took $c \equiv c_{\text{Ni}}$).

Following Carlsson's work [7] we restored two types of interaction: globally and locally relaxed. In the first case it is supposed that the volume of the cluster in the alloy does not depend on the atomic configuration in the cluster. Therefore the set of equations must be solved with the $E_{tot}(c, \Omega, T)$ of the same volume Ω. Hence, it follows that the globally relaxed potentials V_n^g are volume-dependent. In contrast, for a locally relaxed potential it is supposed that the volume of the cluster in alloys is determined by its atomic configuration and in the simplest approximation (which we make here) it is equal to the equilibrium volume of the alloy of the same concentration. Hence, in this case it is necessary to substitute $E_{tot}^0(c, T)$ corresponding to the equilibrium lattice parameter in the set of equations that gives the volume-independent interactions.

In figure 9 we show V_n^g and V_n^l at 0 and 1400 K in comparison with the results of Carlsson and Sanchez [8] (the results of Pasturel *et al* [10] are very close to those of the latter). It can easily be seen that the temperature has very little influence on their values especially in Ni-rich regions. It is quite possible, however, that the Debye–Grüneisen model is too simplified for such high temperatures.

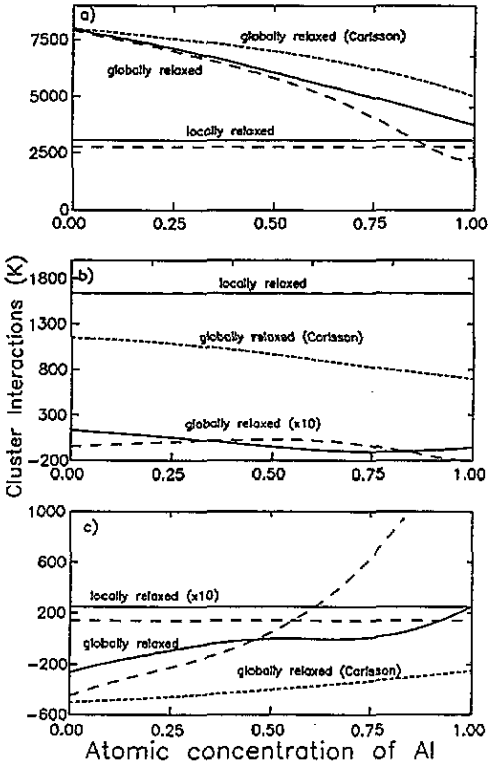

Figure 9. Globally and locally relaxed cluster interactions for the Ni–Al system at 0 K (——) and at 1400 K (– – –). (*a*) Pair interactions (V_2^g, V_2^l); (*b*) triangle interactions (V_3^g, V_3^l); (*c*) tetrahedron interactions (V_4^g, V_4^l). ····· correspond to Carlsson's globally relaxed interactions.

The significant difference between the locally and globally relaxed interactions deserves attention. In particular, V_2^g is more than twice V_2^l and V_3^l is more than an

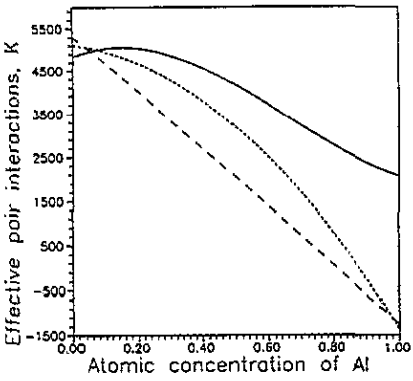

Figure 10. Concentration-dependent globally (——) and locally (– – –) relaxed effective pair interactions at 0 K. ····· is Carlsson's result [7] for locally relaxed pair interactions. The values of the globally relaxed effective pair interactions at each concentration of Al were derived for the corresponding equilibrium volume.

order of magnitude greater than V_3^g. However, it is obvious that direct comparison of these potentials makes no sense, because they arise from different expansions. A comparison with Carlsson's results in that case is more interesting.

First of all let us mention that the values of V_2^g are very close to each other and their dependences on the lattice parameter are similar, though the potentials, obtained in our calculations are a bit smaller than those obtained by Carlsson [8]. At the same time one can see an essential difference between three-and four-atom interactions both in their behaviour and values. In our case, V_3^g is over an order of magnitude less than Carlsson's. Moreover, in contrast to Carlsson's V_3^g our potential has an unexpected minimum for the values of the latter parameter, which correspond to an Al concentration of about 65%. It is difficult to understand such non-monotonic behaviour, considering that this potential actually describes some multisite interaction effects. These effects must evidently correlate with the overlapping integrals, which decrease as the interatomic distance increases. In fact, multisite potentials have part of this information, which is, however, reflected in the general order of values. The potentials' behaviour can be determined by tendencies in the configurational behaviour of alloys. The difference between the results for V_3^g and V_4^g, obtained from various sets of alloy configurations, testifies to a rather bad convergence of the Connolly–Williams (CW) procedure in that case. It can probably be determined also by mistakes in electronic-structure calculations for disordered alloys because of the single-site approximation. The latter describes rather roughly the effects of the local surroundings.

Unfortunately, in [7] the values of locally relaxed interactions are not shown. However, they must be very close to the interactions obtained in this paper because of the closeness of the EPI parameters (see figure 10). In particular, the value of V_2^l is determined by the value of the EPI for pure Ni, the general slope of the curve depends on the value of V_3^l and the deviation from the linear dependence of the EPI is determined by V_4^l. The first two interactions, V_2^l and V_3^l, are in a good agreement with Carlsson's. At the same time, the value of V_4^l obtained by Carlsson must be essentially higher than ours, which is about an order of magnitude less than V_4^g (see figure 9). It is necessary to mention again that the direct comparison of globally and locally relaxed potentials makes no sense. In this case the high value of V_3^l reflects

more an effective concentration dependence of the mixing enthalpy than the values of three-body or configurational interactions.

Generally, from this point of view, it is more convenient to use the globally relaxed interactions for the analysis of ordering effects. In particular, locally relaxed potentials do not allow the evaluation of the influence of ordering effects on the value of the equilibrium lattice parameter because of their volume independence. However this can easily be done with globally relaxed potentials, using either these potentials or EPI parameters, calculated on their basis. Such an evaluation seems very interesting, because diffuse scattering of experimental data in Ni–Al alloys (in the Ni-rich region) [37] shows the existence of strong SRO. Thus, the Cowley–Warren parameters, which are usually determined through pair correlation functions g_i as

$$\alpha_i = (g_i - c^2)/c(1-c) \tag{25}$$

are equal to -0.07 and -0.101 for $T = 673$ K and $c_{Al} = 7.3$ and 10.5 at.% respectively. This is very close to the limit values of $\alpha_i = -c/(1-c)$: -0.078 and -0.117.

In the first order of approximation the SRO energy ΔE_{SRO} for the FCC lattice is expressed through the EPI as

$$\Delta E_{SRO} = 6c(1-c)\alpha_i\phi \tag{26}$$

where ϕ is the EPI on the first shell.

From equation (23) one can see that the existence of SRO in Ni–Al alloy must lead to a general decrease of the energy of the alloy because $\phi > 0$ (see figure 11). Besides this, considering the volume dependence of the EPI (figure 11) in the Ni-rich region we can conclude that SRO effects must lead to the effective decrease of the lattice parameter of alloys with Al concentration greater than 10 at.%, while for alloys of lower Al concentration the lattice parameter must change very slightly. Moreover, as $\Delta E_{SRO} \sim c^2$ ($\alpha_i \to -c/(1-c)$), the existence of SRO in general will lead to a decrease in the slope of the curve of the equilibrium lattice parameters with concentration. It is obvious that in this case the decrease in bulk modulus will become less (figure 7), since the decrease in the lattice parameter will lead to an increase in the electron density on the Wigner–Seitz spheres.

The enthalpy of formation of solid solution is another thermodynamic property which is essentially influenced by SRO effects. For the completely disordered alloy it is calculated directly from the values of full energies obtained by the LMTO–CPA–DFT method. However, for pure components some difficulties arise in our calculation scheme [19]. Another way consists in the calculation of the enthalpy through the CWM. In that case we can also easily take into account the contribution of SRO effects. The results of calculations at $T = 298$ K for all concentrations in the Ni-rich region for the completely disordered solid solution and for the solid solution with SRO are shown in figure 12. To obtain the contribution of SRO effects we minimized the free energy of the alloy over variational parameters in the tetrahedron approximation of the cluster variation method (CVM). Let us mention that the calculated values of the Cowley–Warren parameters are very close to their limit values, which corresponds to the experimental data [37]. The good agreement between the experimental data and theoretical results with the SRO effects taken into account for enthalpies of solid solutions of Al in Ni and Ni_3Al can be seen from figure 12.

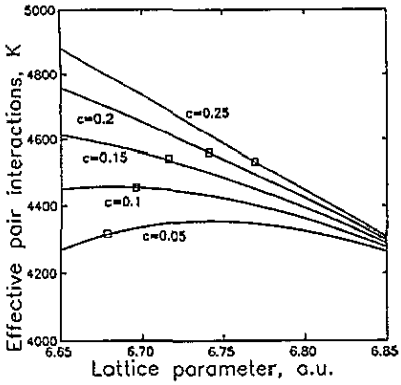

Figure 11. Volume dependence of room-temperature globally relaxed effective pair interactions for different concentration of Al in the Ni-rich region. □ denotes the EPI for the equilibrium lattice constant.

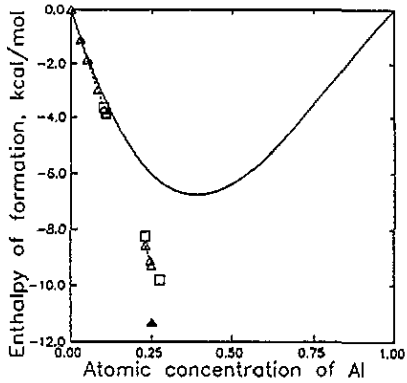

Figure 12. Enthalpies of formation in the Ni–Al system. ——: mixing enthalpy for completely random Ni–Al solid solution; Δ connected by – – –: enthalpy of formation for Ni–Al alloys with short-range order effects and ordered phase Ni_3Al obtained by the CWM; □: corresponding experimental data from [38]; ▲: direct first-principles calculations of enthalpy of formation for Ni_3Al.

It is interesting to consider the Carlsson and Sanchez paper [8], where they calculated the enthalpy of formation of completely disordered solid solutions of Ni–Al in an analogous manner through the CWM on the basis of a set of completely ordered phase energies. Their values of the enthalpies are higher than the corresponding experimental data (for 10 at.% Al $\simeq$ 0.5 kcal mol^{-1}, about 14% of the experimental value). The source of such overestimation is ambiguous. On the one hand, the great difference between our V_3^s and V_4^s and Carlsson's values indicates the insufficiency of the tetrahedron approximation in the CWM for the Ni–Al system. But, on the other hand, the direct calculation of the enthalpy of the ordered Ni_3Al phase (by the programme for compounds) yields a lower value for the latter: -11.4 kcal mol^{-1}, which is, however, in very close agreement with other theoretical calculations: -10.83 kcal mol^{-1} in [4], -11.48 kcal mol^{-1} in [10] and -11.1 kcal mol^{-1} in [39], which is also roughly 15–20% too high. At the same time, if we know the CW interactions, we can easily obtain the enthalpy of formation of the completely ordered phase Ni_3Al. This value (calculated through our CW interactions) is very close to the corresponding experimental result (see figure 12). The reason for such an overestimation of the enthalpy of Ni_3Al in first-principles calculations is not clear yet. However, it is obvious that it must lead to common overestimation of CW interactions and hence to the overestimation of the thermodynamic properties calculated by them.

6. Phase diagram

The possibility of the reproduction of the phase diagram is, however, of the highest interest. Such calculations for the Ni–Al system were done in detail by Carlsson and Sanchez [8], Pasturel *et al* [10] and Lu *et al* [11]. Therefore, it is more interesting for us in this section to show the influence of different approaches in determining cluster interactions on the calculation of a phase diagram. For this purpose we calculated

only the Ni-rich fragment of the phase diagram with both locally and globally relaxed cluster interactions. To obtain the phase boundaries we used the natural iteration method in the CVM, where the free energy of formation was written [40] as

$$F = 2\sum_{ijkl} \epsilon_{ijkl} z_{ijkl} + T\left\{2\sum_{ijkl} L(z_{ijkl}) - 6\sum_{ij} L(y_{ij}) + 5\sum_{i} L(x_i)\right\}$$

$$L(x) = x\ln(x) - x \tag{27}$$

where z_{ijkl}, y_{ij} and x_i are the four-, two- and one-site probabilities of finding the cluster in the $(ijkl)$, (ij) and (i) configurations ($i = 1(2)$ when the site is occupied by an A(B)-type atom). The interaction parameters, ϵ_{ijkl}, used in equation (24), can be expressed through pair potentials ϵ_{12} and parameters a and b, which contain the contribution of multisite interactions in the following form

$$\epsilon_{1112} = \tfrac{3}{2}\epsilon_{12}(1+a) \qquad \epsilon_{1122} = 2\epsilon_{12} \qquad \epsilon_{1222} = \tfrac{3}{2}\epsilon_{12}(1+b). \tag{28}$$

These parameters are expressed through CW interactions as

$$\epsilon_{12} = -\tfrac{1}{3}V_2 \qquad a = (2V_4 - V_3)/V_2 \qquad b = (2V_4 + V_3)/V_2. \tag{29}$$

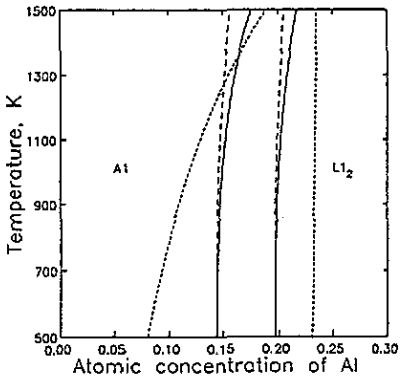

Figure 13. The fragment of the Ni–Al phase diagram in the Ni-rich corner. Theoretical boundaries of solubility are shown by —— for globally relaxed interactions and – – – for locally relaxed interactions. The experimental boundaries of solubility are designated by ·····.

The greatest difference between calculations with globally and locally relaxed interactions lies in the high-temperature region (figure 13). The result, which corresponds to the globally relaxed potential, agrees better with experimental data. The region of two-phase equilibrium in both cases at $T = \frac{1}{2}T_c$ (where $T_c = 1847$ K is the computed ordering temperature) is about 6 at.%, which agrees well with Carlsson's results [8] and is about two times less than the corresponding experimental data. In spite of the essential deviation of CW potentials (in particular in V_3^g, obtained in our calculations and by Carlsson [8]), there is, in general, good agreement between phase diagrams reproduced. In addition, our calculations show that the phase diagram is practically insensitive to the temperature dependence of the potentials. Taking into

consideration that the calculated enthalpy of formation is in good agreement with the experimental one, we can conclude that the biggest error in the phase diagram reproduction is contained in the calculation of the entropy within the tetrahedron approximation in the CVM. It is also indirectly proved by Carlsson's results [8] for the transition temperature and free energy, which are about 40% higher than the experimental ones, though the error in the calculated enthalpy of formation is only about 20%.

To verify this conclusion we also calculated the free energy of formation at 1273 K at the Ni-rich end for an FCC solid solution by the CVM. The results are presented in table 4. In contrast to the enthalpy of formation (figure 12) in this case we found a deviation of about 20% from the experimental data, the temperature dependence of interactions having almost no influence on the results. Thus, in our calculation of the free energy of formation we incurred an additional error of about 20% in comparison with enthalpy of formation, as is the case in [8].

Table 4. Free energy of formation for Ni–Al solid solution at 1273 K (in kcal mol^{-1}). Experimental values taken from [38].

c_{Al} (at.%)	ΔF_{calc}	ΔF_{exp}
5	−2.31	−2.12
10	−4.33	−3.85
14.3	−5.87	−5.09

7. Conclusions

In this study we have applied the fast LMTO–CPA method together with density functional theory to calculate the electronic structure, thermal and thermodynamic properties of Ni–Al random alloys. First of all we have revealed that the hybridization between p electrons of Al and d electrons of Ni reduces with Al concentration and disordering in the Ni-rich region. In our view in both cases this fact is related directly to the change in the atomic configuration. In particular, the hybridization increases when Al atoms are surrounded by atoms of Ni. The additional hybridization with ordering implies the increase of covalent contribution to the interatomic forces and, consequently, the general decrease of the energy of an alloy. Thus, the nature of strong short-range order effects in Ni-rich alloy becomes clear.

To calculate the thermodynamic properties of the Ni–Al system we have used the Connolly–Williams method, which has been applied earlier by Carlsson and co-workers to this system but on the basis of total energy-band calculations of elements and ordered phases. Although our results for the thermodynamic properties and phase diagram are in close agreement with Carlsson's we have found strong differences between the corresponding globally and locally relaxed interactions, in particular for V_3^g, V_4^g and V_4^l. It is possible that this discrepancy arises from the insufficient convergency of the tetrahedron truncation in the CWM. But we cannot exclude the error coming from the single-site approximation in our LMTO–CPA calculations which is reflected in the difference between the values of the enthalpy of formation of the ordered Ni_3Al phase calculated by the LMTO–CPA and the ordinary LMTO method.

It is also very interesting that the temperature-dependence of the interaction parameters, enthalpy and free energy of formation, as well as the phase diagram, accounted for by the Debye–Grüneisen analysis of the binding curves, is very slight, and the greatest error arising in calculations of the free energy of formation and the phase diagram is the result of the lack of accuracy in the entropy calculation by the tetrahedron approximation in the CVM.

Acknowledgment

One of us (IAA) would like to thank Dr H L Skriver for his hospitality at the Technical University of Denmark, where some of the present results were obtained.

References

[1] Johonson D D, Nicholson D M, Pinsky F J, Gyorffy B L and Stocks G M 1990 *Phys. Rev.* B **41** 9701
[2] Johonson D D, Nicholson D M, Pinsky F J, Gyorffy B L and Stocks G M 1986 *Phys. Rev. Lett.* **56** 2088
[3] Abrikosov I A, Vekilov Yu H and Ruban A V 1991 *Phys. Lett.* A **154** 407
[4] Hackenbracht D and Kübler J 1980 *J. Phys. F: Met. Phys.* **10** 427
[5] Miedema A R, Chatel P F and de Boer F R 1980 *Physica* B **100** 1
[6] Connolly J W D and Williams A R 1983 *Phys. Rev.* B **27** 5169
[7] Carlsson A E 1987 *Phys. Rev.* B **35** 4858
[8] Carlsson A E and Sanchez J M 1988 *Solid State Commun.* **65** 527
[9] Carlsson A E 1989 *Phys. Rev.* B **40** 912
[10] Pasturel A, Colinet C, Paxton A T and van Schilfgaarde M 1992 *J. Phys.: Condens. Matter* **4** 945
[11] Lu Z W, Wei S-H, Zunger A, Frota-Pessoa S and Ferreira L G 1991 *Phys. Rev.* B **44** 512
[12] Moruzzi V L, Janak J F and Schwarz K 1988 *Phys. Rev.* B **37** 790
[13] Sanchez J M, Stark J P and Moruzzi V L 1991 *Phys. Rev.* B **44** 5411
[14] Gyorffy B L 1972 *Phys. Rev.* B **5** 2382
[15] Gordon B E A, Temmerman W E and Gyorffy B L 1981 *J. Phys. F: Met. Phys.* **11** 821
[16] Gunnarson O, Jepsen O and Andersen O K 1983 *Phys. Rev.* B **27** 7144
[17] Andersen O K, Pawlowska Z and Jepsen O 1986 *Phys. Rev.* B **34** 5253
[18] Akai H 1989 *J. Phys.: Condens. Matter* **1** 8045
[19] Abrikosov I A, Vekilov Yu H, Ruban A V and Katz D Ya 1991 *Solid State Commun.* **80** 177
[20] Zeller R, Deutz J and Dederichs P H 1982 *Solid State Commun.* **44** 993
[21] Perdew J P and Zunger A 1981 *Phys. Rev.* B **23** 5048
[22] Steiner P, Hochst H, Steffen W and Hufner S 1980 *Z. Phys.* B **38** 191
[23] Deutz J, Dederichs P H and Zeller R 1981 *J. Phys. F: Met. Phys.* **11** 1787
[24] Wenger A, Burri G and Steineman S 1971 *Solid State Commun.* **9** 1125
[25] Sluiter M and Turchi P E A 1989 *Phys. Rev.* B **40** 11215
[26] Vinet P, Rose J H, Ferrante J and Smith J R 1989 *J. Phys.: Condens. Matter* **1** 1941
[27] Foiles S M and Daw M S 1987 *J. Mater. Res.* **2** 5
[28] Barron T H K 1955 *Phil. Mag.* **46** 720
[29] Pearson W B 1967 *A Handbook of Lattice Spacing and Structure of Metals and Alloys* (London: Pergamon)
[30] Rao P V H, Suryanarayana S V, Satyanarayna Murthy K and Nagender Naidu S V 1989 *J. Phys.: Condens. Matter* **1** 5357
[31] Fisher E S 1986 *Scr. Metall.* **20** 279
[32] Ono K and Stern R 1968 *Trans. AIME* **245** 171
[33] Dickson R W, Wachtman J B and Copely S M 1969 *J. Appl. Phys.* **40** 2276
[34] Kayser F X and Stassis C 1981 *Phys. Status Solidi* a **64** 335
[35] Wallow F, Neite G, Schroer W and Nembach E 1987 *Phys. Status Solidi* a **99** 483
[36] Kornilov I I and Minz R S 1963 *Dokl. Akad. Nauk USSR* **88** 129

[37] Chassagne F, Bessiere M, Calvayrac Y, Cenedese P and Lefebvre S 1989 *Acta Metall.* **37** 2329
[38] Hultgren R, Desai P D, Hawkins D T, Gleiser M and Kelley K K 1973 *Selected Values of Thermodynamic Properties of Binary Alloys* (Metals Park, OH: American Society for Metals)
[39] Xu J-H, Oguchi T and Freeman A J 1987 *Phys. Rev.* B **36** 4186
[40] Kikuchi R and Murray J 1985 *CALPHAD* **9** 311